Episodes of intensified biological productivity in the subtropical Atlantic Ocean during the termination of the Middle Eocene Climatic Optimum (MECO)

AGU PUBLICATIONS

Paleoceanography

RESEARCH ARTICLE
10.1002/2014PA002673

Key Points:
- Two higher-productivity intervals (HPIs) at peak MECO and shortly after the MECO
- HPIs attributed to strengthened hydrological cycle and enhanced runoff
- HPIs appear to correlate with similar events in other ocean basins

Supporting Information:
- Figure S1
- Data Set S1
- Data Set S2

Correspondence to:
I. Moebius,
moebius@em.uni-frankfurt.de

Citation:
Moebius, I., O. Friedrich, K. M. Edgar, and P. F. Sexton (2015), Episodes of intensified biological productivity in the subtropical Atlantic Ocean during the termination of the Middle Eocene Climatic Optimum (MECO), *Paleoceanography*, *30*, doi:10.1002/2014PA002673.

Received 21 MAY 2014
Accepted 6 JUL 2015
Accepted article online 14 JUL 2015

Episodes of intensified biological productivity in the subtropical Atlantic Ocean during the termination of the Middle Eocene Climatic Optimum (MECO)

Iris Moebius[1,2], Oliver Friedrich[3], Kirsty M. Edgar[4,5], and Philip F. Sexton[6]

[1]Now at Department of Earth and Environmental Sciences, Lamont-Doherty Earth Observatory of Columbia University, New York, USA, [2]Institut für Geowissenschaften, Goethe-Universität Frankfurt, Frankfurt, Germany, [3]Institut für Geowissenschaften, Universität Heidelberg, Heidelberg, Germany, [4]Now at School of Earth Sciences, University of Bristol, Bristol, UK, [5]School of Earth and Ocean Sciences, Cardiff University, Cardiff, UK, [6]Centre for Earth, Planetary, Space and Astronomical Research, Open University, Milton Keynes, UK

Abstract The Middle Eocene Climatic Optimum (MECO) is an ~500 kyr interval of pronounced global warming from which the climate system recovered in <50 kyr. The deep-sea sedimentary record can provide valuable insight on the marine ecosystem response to this protracted global warming event and consequently on the ecological changes during this time. Here we present new benthic foraminiferal assemblage data from Ocean Drilling Program Site 1051 in the subtropical North Atlantic, spanning the MECO and post-MECO interval (41.1 to 39.5 Ma). We find little change in the species composition of benthic foraminiferal assemblages during the studied interval, suggesting that the rate of environmental change was gradual enough that these organisms were able to adapt. However, we identify two transient intervals associated with peak warming (higher-productivity interval (HPI)-1; 40.07–39.96 Ma) and shortly after the MECO (HPI-2; 39.68–39.55 Ma), where benthic foraminiferal accumulation rates increase by an order of magnitude. These HPIs at Site 1051 appear to coincide with intervals of strengthened productivity in the Tethys, Southern Ocean, and South Atlantic, and we suggest that an intensified hydrological cycle during the climatic warmth of the MECO was responsible for eutrophication of marine shelf and slope environments.

1. Introduction

The Eocene (56 to 34 Ma) is characterized by significant global climate change. Following the pronounced warming event at the Paleocene-Eocene boundary (Paleocene-Eocene Thermal Maximum (PETM) [e.g., *Zachos et al.*, 2008]) at ~56 Ma [*Westerhold et al.*, 2009], a global greenhouse climate persisted during the early Eocene (56–50 Ma), with background deep-ocean temperatures reaching 14°C [*Sexton et al.*, 2006; *Zachos et al.*, 2008] and sea surface temperatures of 28–35°C [e.g., *Bijl et al.*, 2009; *Burgess et al.*, 2008; *Hollis et al.*, 2009; *Pearson et al.*, 2001, 2007]. Thereafter, a gradual cooling took place during the middle and late Eocene (49–34 Ma) [*Cramer et al.*, 2009; *Sexton et al.*, 2006; *Zachos et al.*, 2008] culminating in the growth of the first continental-scale ice caps across Antarctica during the Eocene-Oligocene transition [*Coxall et al.*, 2005; *Miller et al.*, 1991; *Zachos et al.*, 1996]. Superimposed on this long-term Eocene climate evolution are a series of transient global warming events. These include the short-lived (<200 kyr in duration) "hyperthermals" such as the PETM and other, more modest events that pepper the early and middle Eocene (including, for example, the Eocene Thermal Maximums 2 and 3 (ETM-2 and ETM-3, respectively) [*Kennett and Stott*, 1991; *Lourens et al.*, 2005; *Sexton et al.*, 2011; *Sluijs et al.*, 2009; *Thomas and Shackleton*, 1996; *Zachos et al.*, 2001, 2003] as well as longer-lived warming events such as the Middle Eocene Climatic Optimum (MECO) [e.g., *Bohaty and Zachos*, 2003; *Bohaty et al.*, 2009]. The latter is a prominent ~500 kyr long warming event that interrupts the middle to late Eocene cooling trend at ~40 Ma. The $\delta^{18}O$ records from bulk sediment and benthic foraminiferal calcite indicate a gradual decrease of 1.0–1.5‰ during the MECO [*Bohaty and Zachos*, 2003; *Bohaty et al.*, 2009; *Edgar et al.*, 2010; *Sexton et al.*, 2006]. Assuming an absence of significant continental ice sheets at that time [*Bijl et al.*, 2010; *Burgess et al.*, 2008; *Edgar et al.*, 2007], this $\delta^{18}O$ shift likely represents a temperature increase of 4–6°C in surface and deep waters [*Bohaty and Zachos*, 2003; *Bohaty et al.*, 2009; *Edgar et al.*, 2010; *Sexton et al.*, 2006]. This is consistent with estimates from independent temperature proxies such as TEX_{86} and U^{K}_{37}, suggesting high-latitude sea surface warming of 3°C to 6°C during the MECO [*Bijl et al.*, 2010; *Boscolo Galazzo et al.*, 2014]. Inferred ocean warming culminates

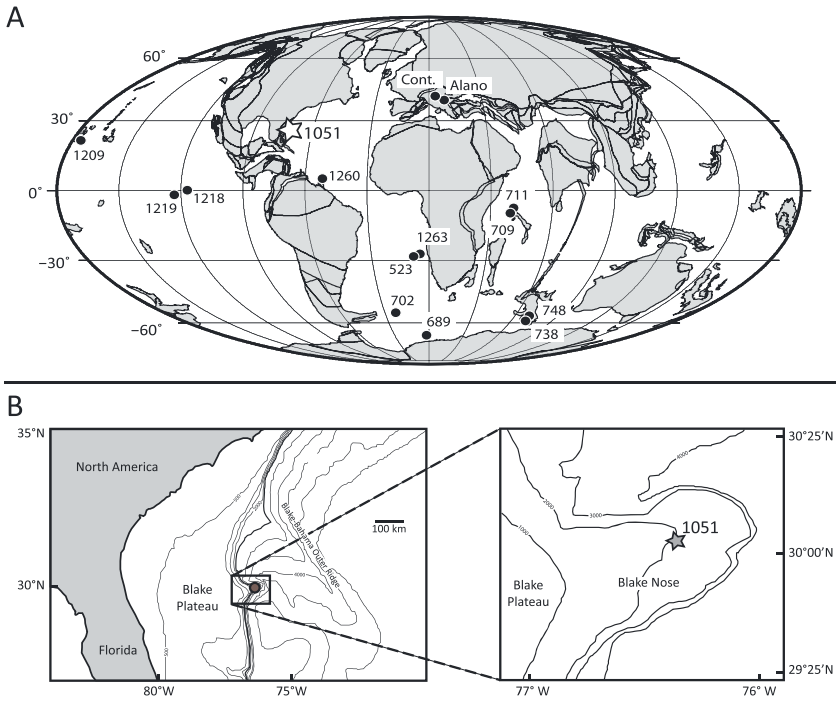

Figure 1. Study site. (a) Paleogeographic map of the middle Eocene (40 Ma reconstruction; after http://www.odsn.de [*Hay et al.*, 1999]). ODP Site 1051 (this study) is indicated by the red star. The blue circles show the positions of all sites where MECO records are published. Assumptions about paleoproductivity are summarized in Table 2. (b) Present-day bathymetric map showing the location of ODP Site 1051, drilled during Leg 171b on the Blake Nose plateau [after *Norris et al.*, 1998].

in a δ^{18}O minima (i.e., MECO peak warming) lasting ~50 kyr at ~40.0 Ma [*Bohaty et al.*, 2009; *Edgar et al.*, 2010]. The MECO is also accompanied by a transient increase in atmospheric pCO_2 [*Bijl et al.*, 2010] as well as a brief, ~500 to 1500 m global shoaling of the carbonate compensation depth (CCD) [*Bohaty et al.*, 2009; *Pälike et al.*, 2012].

In contrast to preceding early Eocene hyperthermals [*Lourens et al.*, 2005; *Nicolo et al.*, 2007; *Sexton et al.*, 2011; *Zachos et al.*, 2010], the MECO is not accompanied by a contemporaneous negative δ^{13}C excursion. However, a small and brief negative δ^{13}C excursion (~0.5‰) does occur coincident with inferred peak warming near the termination of the MECO (~40.0 Ma) [e.g., *Bohaty et al.*, 2009; *Boscolo Galazzo et al.*, 2014; *Edgar et al.*, 2010]. This apparent absence of large-scale injection of isotopically depleted carbon into the middepth to upper depth ocean and atmosphere suggests that the mechanism responsible for the MECO differs from that of the earlier Eocene hyperthermals, for which methane hydrate dissociation [e.g., *Dickens et al.*, 1995; *Lourens et al.*, 2005; *Lunt et al.*, 2011], peatland-derived organic carbon [*Higgins and Schrag*, 2006; *Kurtz et al.*, 2003], oceanic dissolved organic carbon [*Sexton et al.*, 2011], permafrost organic carbon [*DeConto et al.*, 2012], carbon release through heating of carbon-rich sediments associated with the intrusion of magmatic sills [*Svensen et al.*, 2004], and volcanic degassing [*Eldholm and Thomas*, 1993; *Maclennan and Jones*, 2006] have been invoked. In contrast, the gradual warming and coincident CCD shoaling during the MECO are more likely attributable to a progressive increase in pCO_2 as a result of extensive arc or ridge volcanism and/or a pulse of metamorphism associated with the Himalayan orogeny [*Bijl et al.*, 2010; *Bohaty and Zachos*, 2003]. However, it is difficult to reconcile these observations, the existing carbon cycle theory, because over the time scales of MECO warming, continental weathering should have increased and acted to increase ocean carbonate saturation state and thus deepen (and not shoal) the CCD [*Sluijs et al.*, 2013].

The termination of the MECO is marked by an abrupt positive δ^{18}O shift indicating cooling of ~6°C in surface and intermediate deep waters within as little as 50 kyr [*Bohaty et al.*, 2009]. This rapid cooling was accompanied by a global deepening of the CCD [*Bohaty et al.*, 2009] and a rapid decrease in pCO_2 [*Bijl et al.*, 2010]. Weathering of silicate rocks can draw down pCO_2 on time scales of 10^5 years. However, the termination of the MECO and suggested pCO_2 decrease occurred within $<$50 kyr [*Bohaty et al.*, 2009],

pointing to changes in carbon cycling within Earth's surficial reservoirs (ocean, atmosphere, and biosphere) as the most likely candidate for pCO_2 drawdown, with intensified silicate weathering rates being a possible additional (smaller) contributory process [*Pälike et al.*, 2012].

Here we used samples from Ocean Drilling Program (ODP) Site 1051 to evaluate the impact of this pronounced global warming event on the marine ecosystem in the subtropical western North Atlantic (Blake Plateau; star in Figure 1a). Site 1051 is stratigraphically continuous (at least to biozone and magnetozone levels), has high-resolution bulk carbonate stable isotope data across the MECO [*Bohaty et al.*, 2009; *Edgar et al.*, 2010], and a well-defined magnetostratigraphy and age model [*Edgar et al.*, 2010]. We use benthic foraminiferal assemblages, as well as benthic and planktic foraminifera accumulation rates (BFAR and PFAR) to reconstruct paleoproductivity variations at this site.

Our data document changes in benthic foraminifera assemblages across the MECO and determine whether there is any evidence for intervals of elevated productivity in the North Atlantic Ocean during the MECO. We then compare our results to those from other locations to evaluate the geographic extent of inferred eutrophication during the MECO interval.

2. Material and Methods

2.1. Site Location and Material

Site 1051 was drilled during ODP Leg 171B along a depth transect on Blake Nose (30°03′N, 76°21′W; Figure 1b), a topographic high off the coast of Florida that extends eastward with a gentle slope into the North Atlantic from Blake Plateau. Site 1051 has a modern water depth of 1980 m below sea level. Sediments were deposited at an estimated middle Eocene paleowater depth of ~1000–2000 m [*Norris et al.*, 1998] at ~25°N paleolatitude [*Ogg and Bardot*, 2001]. The cores recovered from two holes constitute a stratigraphically complete upper Eocene to lower Paleocene succession composed of calcareous or siliceous ooze, chalk, and clay, interspersed by 25 thin layers of volcanic ash [*Norris et al.*, 1998]. Sediments were deposited above the local CCD throughout the study interval and are shallowly buried ($<$150 m), providing "good" (albeit recrystallized) preservation of calcareous microfossils [*Edgar et al.*, 2010, 2013]. Eocene sediments consist of a yellow, siliceous nannofossil ooze (subunit 1C), underlain by green nannofossil ooze (subunit 1D) [*Norris et al.*, 1998]. The sharp color change marks the transition between the subunits, but the sediment composition mainly remains the same.

2.2. Sample Preparation

For benthic foraminiferal assemblages, a total of 52 samples have been taken across the MECO following the shipboard-spliced sequence [*Norris et al.*, 1998] between 60 and 130 meters composite depth (mcd): 1 m sampling resolution across the MECO (80–115 mcd), 2 m spacing outside of the event (115–130 mcd and 60–80 mcd, respectively), and decreased sample spacing down to 20 cm during two intervals following the MECO (68–70 mcd and 80–87 mcd). This results in a temporal resolution of 4 to 40 kyr for the benthic foraminiferal assemblage data. All sediment samples were initially dried and weighed before being disaggregated in distilled water and washed through a 63 μm sieve.

Benthic foraminiferal assemblage counts are based on the $>$125 μm size fraction. If more than 250–300 specimens were present in a single sample, representative splits of the sample material were counted. Benthic foraminiferal numbers are then recalculated for the entire sample and are presented as the number of individuals per gram (n/g) of dry sediment (Figure 2). It is common practice in paleoecological studies to count up to 300 specimens per sample to ensure that the results are statistically significant. However, in most samples even counting the entire $>$125 μm size fraction (rather than a split) it was not possible to reach 300 specimens (supporting information). Accordingly, a notable statistical error is likely for interpretations that are based on abundances composition. Classification was carried out to the species level whenever possible and mainly followed *Bolli et al.* [1994] and *Tjalsma and Lohmann* [1983].

From comparison with published data on fossil and recent benthic foraminiferal communities, the most common genera in the assemblages were allocated to probable ecological habitats (Table 1). These habitats are primarily characterized by differences in bottom water oxygenation as well as nutrient supply to the seafloor and seasonality. Benthic foraminiferal assemblage data thus provide information on bottom

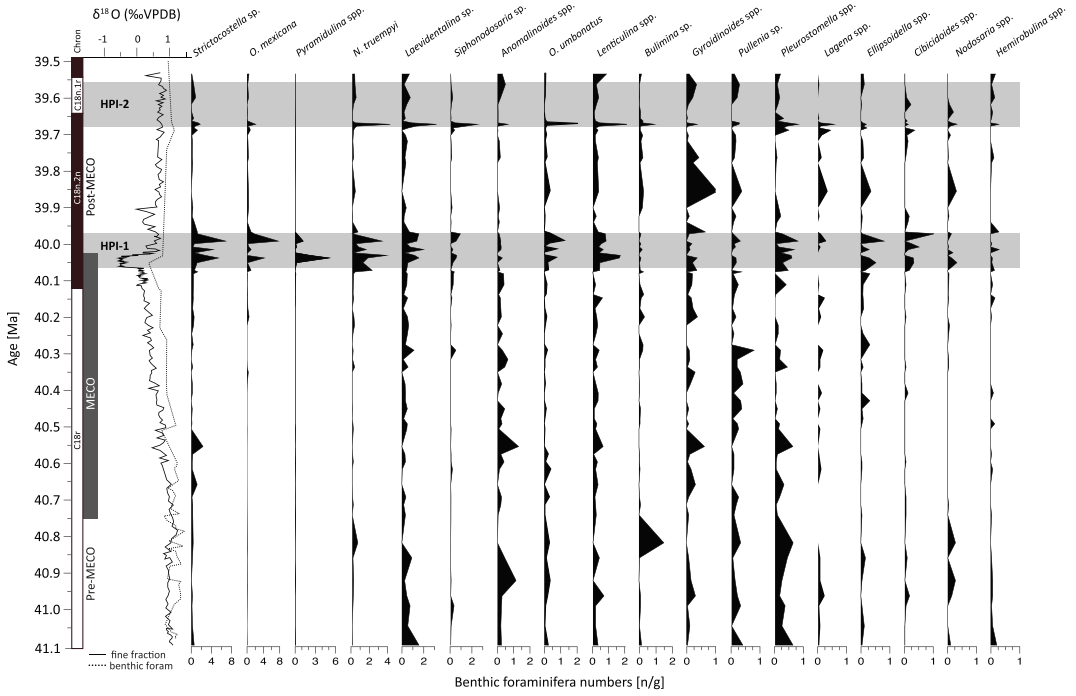

Figure 2. The δ^{18}O records and benthic foraminiferal numbers at ODP Site 1051. Most benthic taxa show little variation in relative abundance throughout the investigated section (41.1–39.5 Ma), except for two brief intervals (highlighted in gray) at ~40 Ma (MECO peak warming) and ~39.65 Ma (post-MECO). Fine-fraction isotope data (solid line) are from *Bohaty et al.* [2009], and benthic foraminiferal isotope data (dotted line) are from *Edgar et al.* [2010].

water characteristics, specifically oxygenation and the flux of organic matter to the seafloor [e.g., *Jorissen et al*., 2007; *Murray*, 2001].

Planktic foraminiferal abundances are, like most planktic dwellers, dependent on food supply and nutrient input, while benthic foraminiferal accumulation rates (BFARs) are well correlated to export, and even primary, productivity [e.g., *Herguera and Berger*, 1991; *Jorissen et al*., 2007; *Van der Zwaan et al*., 1999]. BFARs were calculated following *Herguera and Berger* [1991]:

$$\mathrm{BFAR} = \mathrm{F}\cdot\mathrm{LSR}\cdot\mathrm{DBS}\left[\mathrm{n/cm^2/kyr}\right]$$

where F is the benthic foraminifera abundance (n/g), LSR is the linear sedimentation rate (cm/kyr), and DBS is the dry bulk sediment (g/cm^3) (g = grams of dry sediment).

Planktonic foraminifera were analyzed only for total abundances in representative sample splits, allowing for a much higher sample resolution of 10 cm spacing between 60 and 102 mcd, resulting in a total of 296 samples. This encompasses the majority of the MECO and post-MECO intervals. Counts were made on a representative split of the >300 μm size fraction comprising >300 individuals. Following *Van Kreveld* [1997], PFARs were calculated using the same formula as for BFAR (see above).

2.3. Weight %$CaCO_3$

A high-resolution record of estimated bulk weight %$CaCO_3$ was generated for our study interval to evaluate any changes in carbonate preservation that may bias our records. Estimates were calculated by developing a regression between the high-resolution physical property parameter—lightness (L^*) and discrete shipboard $CaCO_3$ measurements by *Norris et al.* [1998] ($R^2 = 0.85$). Prior to plotting, a Gaussian filter with a 20 cm window was applied to L^* data to increase the signal-to-noise ratio.

2.4. Age Model

The age model employed in this study is based on the revised ODP Site 1051 magnetostratigraphy by *Edgar et al.* [2010]. The uncertainty in the determination of the magnetochron boundaries is low and varies from ±1 cm (<1 kyr) for the base of magnetochrons C19n, C18r, to C18n.1r to ±55 cm for the base of C18n.2n

Table 1. Ecological Preference of All Taxa That Take Up >1% of the Assemblage[a]

Taxon	Microhabitat	Source	Preferred ecology	Source
Anomalinoides	Cretaceous: epifaunal	*Thomas* [1990]	Recent: oligotrophic to mesotrophic and rather well-ventilated conditions	*Badawi et al.* [2005] and *Jorissen et al.* [1995]
	Miocene: epifaunal	*Smart et al.* [2007]		
	K/P boundary: epifaunal	*Peryt et al.* [2002]		
	Paleocene: epifaunal	*Oberhänsli et al.* [1991]		
	Recent: epifaunal	*Alegret et al.* [2009]		
Bulimina	K/P boundary: infaunal	*Peryt et al.* [2002] and *Alegret and Thomas* [2005]	Recent: common in oxygen minimum zones and/or areas of high organic mater input	*Gooday* [2003] and *Schmiedl et al.* [1997]
	Miocene: infaunal	*Petrová* [2004]		
	Recent: infaunal	*Rosoff and Corliss* [1992]		
			Miocene: dysoxic-suboxic	*Petrová* [2004]
			PETM: low oxygen and/or high organic matter	*Thomas* [2003]
Cibicidioides	PETM: epifaunal	*Alegret and Thomas* [2004]	Recent: oligotrophic, well oxygenated, and low TOC	*Badawi et al.* [2003] and *Jorissen et al.* [2007]
	Recent: epifaunal to very shallow infaunal	*Badawi et al.* [2005], *Linke and Lutze* [1993], *Corliss* [1991], and *Jorissen et al.* [2007]		
	Cretaceous: epifaunal	*Friedrich et al.* [2006]		
Ellipsoidella	No literature available		No literature available	
Gyroidinoides	Cretaceous: epifaunal	*Thomas* [1990]	Recent: suboxic	*Kaiho* [1999]
	Miocene: epifaunal	*Smart et al.* [2007]	Cretaceous: mesotrophic, intolerant to dysoxic conditions	*Friedrich and Erbacher* [2006] and *Erbacher et al.* [1999]
	K/P boundary: epifaunal	*Peryt et al.* [2002]		
	Laboratory experiments: shallow infaunal	*Erbacher et al.* [1998]		
Hemirobulina	No literature available		No literature available	
Laevidentalina	K/P boundary: infaunal	*Peryt et al.* [2002] and *Alegret and Thomas* [2005]	K/P boundary: oligotroph	*Peryt et al.* [2002]
	PETM: infaunal	*Alegret et al.* [2009]	Cretaceous: tolerant of oxygen depletion in bottom waters and high organic flux, associated with black shale	*Friedrich and Erbacher* [2006] and *Kaiho and Hasegawa* [1994]
Lagena	Recent: infaunal	*Rosoff and Corliss* [1992]	Recent: suboxic	*Kaiho* [1999]
			Miocene: suboxic	*Petrová* [2004]
Lenticulina	Miocene: epifaunal	*Smart et al.* [2007]	Cretaceous: dysoxic, low-oxygen tolerant, associated with black shales, tolerance of dysoxia	*Friedrich et al.* [2003], *Friedrich* [2010], and *Friedrich et al.* [2006]
	Recent: epifaunal, infaunal, and shallow infaunal	*Rosoff and Corliss* [1992], *Gooday* [2003], *Corliss* [1991], and *Den Dulk et al.* [2000]		
	K/P boundary: epifaunal	*Peryt et al.* [2002]	PETM: capable of alternating between an epibenthic and shallow endobenthic lifestyles in reaction to low-oxygen, eutrophic conditions	*Stassen et al.* [2012], *Coccioni and Galeotti* [1993], and *Nyong and Ramanathan* [1985]
	Cretaceous: possibly deep infaunal	*Friedrich et al.* [2006]		
			Miocene: suboxic	*Petrová* [2004]
			Recent: suboxic	*Kaiho* [1999]
Nodosaria	Elongate morphology -> infaunal according to	*Corliss* [1991]	PETM: adapted to normal marine conditions	*Stassen et al.* [2012]
			Cretaceous: low to moderate oxygen depletion	*Koutsoukos et al.* [1990]
			Eocene: anaerobic	*Kaiho* [1991]
N. truempyi	PETM: epifaunal	*Alegret and Thomas* [2004] and *Takeda and Kaiho* [2007]	Eocene: indicative of oligotrophic conditions, intolerant to ocean acidification, well oxygenated	*Thomas et al.* [2000] and *Müller-Merz and Oberhänsli* [1991]
	Eocene: epifaunal	*Boscolo Galazzo et al.* [2013]		
			PETM: oligotrophic indicator	*Takeda and Kaiho* [2007] and *Mancin et al.* [2013]

Table 1. (continued)

Taxon	Microhabitat	Source	Preferred ecology	Source
			Cretaceous: oligotrophic, well oxygenated	*Friedrich and Erbacher* [2006], *Schoenfeld and Burnett* [1991], and *Widmark and Speijer* [1997]
O. umbonatus	Neogene: shallow infaunal	*Bhaumik et al.* [2011]	Recent: well oxygenated, low organic matter flux	*Mackensen et al.* [1985] and *Gooday* [2003]
	Recent: epifaunal	*Den Dulk et al.* [2000] and *Corliss and Chen* [1988]		
Osangularia or spec. *O. mexicana*	K/P boundary: epifaunal	*Alegret and Thomas* [2005]	Cretaceous: opportunistic, associated with reventilation during black-shale formation, able to withstand hypoxia	*Friedrich et al.* [2005] and *Friedrich et al.* [2006]
	Eocene: epifaunal	*Oberhänsli et al.* [1991]		
	Recent: epifaunal	*Corliss and Chen* [1988]		
Pleurostomella	Pleistocene: infaunal	*Kaiho* [1992a, 1992b]	Pleistocene: low oxygen and/or high organic matter	*Kaiho* [1992a, 1992b]
Pullenia	Recent: infaunal and shallow infaunal	*Rosoff and Corliss* [1992] and *Den Dulk et al.* [2000]	Miocene: suboxic	*Petrová* [2004]
	Cretaceous: infaunal	*Thomas* [1990]	Recent: low oxygen, high organic matter, suboxic	*Gooday* [1994] and *Kaiho* [1999]
Pyramildulina	Cretaceous: epifaunal and shallow infaunal	*Shackleton et al.* [1984], *Koutsoukos and Hart* [1990], and *Fassell and Bralower* [1999]	No literature data available	
Siphonodosaria	Elongate morphology -> infaunal according to	*Oberhänsli et al.* [1991] and *Corliss* [1991]	Miocene: anoxic to dysoxic	*Petrová* [2004]
Strictocostella	K/P boundary: infaunal	*Kaiho* [1992a, 1992b]	K/P boundary: anaerobic	*Kaiho* [1992a, 1992b]
	Miocene: infaunal	*Petrová* [2004]	Miocene: anoxic-dysoxic	*Petrová* [2004] and *Drinia et al.* [2003]

[a]Name of species or genus is given in column 1, column 2 presents the assumed habitat (infaunal, shallow infaunal, and epifaunal) with references in column 3, and column 4 describes the ecological preference with respect to nutrient and oxygen availability with references in column 5. Time period or epoch of the specimen investigated in the cited studies is also indicated.

(maximum uncertainty of ~38 kyr). All ages are reported on the time scale of *Cande and Kent* [1995]. Accumulation rates are calculated by assuming that sedimentation rates remained constant between magnetochron datums; estimated sedimentation rates vary between ~2 and 6 cm/kyr (Figure 3f). Unfortunately, an orbital chronology is not currently available for this site, and biostratigraphy does not provide any additional constraints due to large offsets that imply that further calibration of the existing biostratigraphic datums is required [see *Edgar et al.*, 2010].

3. Results and Discussion

The middle Eocene of Site 1051 is characterized by low total organic carbon (TOC) values throughout the investigated succession (0.06 wt % on average) [*Norris et al.*, 1998], while $\%CaCO_3$ values are relatively high. Weight $\%CaCO_3$ values average ~74% in the lower part of the succession but increase abruptly to ~82% at 39.78 Ma, above the MECO (Figure 3e). This step change in $\%CaCO_3$ is not reflected in any other chemical proxy but is accompanied by a pronounced change in sediment color from pale yellow to grayish green [*Norris et al.*, 1998]. This color change obviously impacts measured L^* values (Figure 3e) and thus the estimated $\%CaCO_3$ values (see section 2.4). Regardless, the continuously high $CaCO_3$ (and lack of physical evidence for a dissolution horizon in the sediments) during the MECO itself suggests that Site 1051 was likely situated above the local lysocline and CCD. Thus, the sediments were, similar to other shallow sites, not subject to extensive dissolution even during the peak of the MECO, as is observed at sites situated below 3000 m paleowater depth [*Bohaty et al.*, 2009; *Pälike et al.*, 2012].

Benthic foraminiferal assemblages at ODP Site 1051 are diverse, and their good preservation state enables identification of foraminifera to the species level. A total of 48 benthic foraminiferal taxa were identified (Figure 2), with 20 genera having an average relative abundance of >1% in the samples. The most common species (>5% of the total assemblage) are *Anomalinoides* spp. (including *A. alazanensis*, *A. subbadenensis*, and *A. pompilioides*), *Gyroidinoides* spp. (including *G. complanatus*, *G. planulatus*, and *G. girardanus*), *Laevidentalina* spp. (including *L. legumen*, *L. gracilis*, *L. communis*, and *L. spinescens*), *Lenticulina* spp. (*L. lepida*, *L. muensteri*,

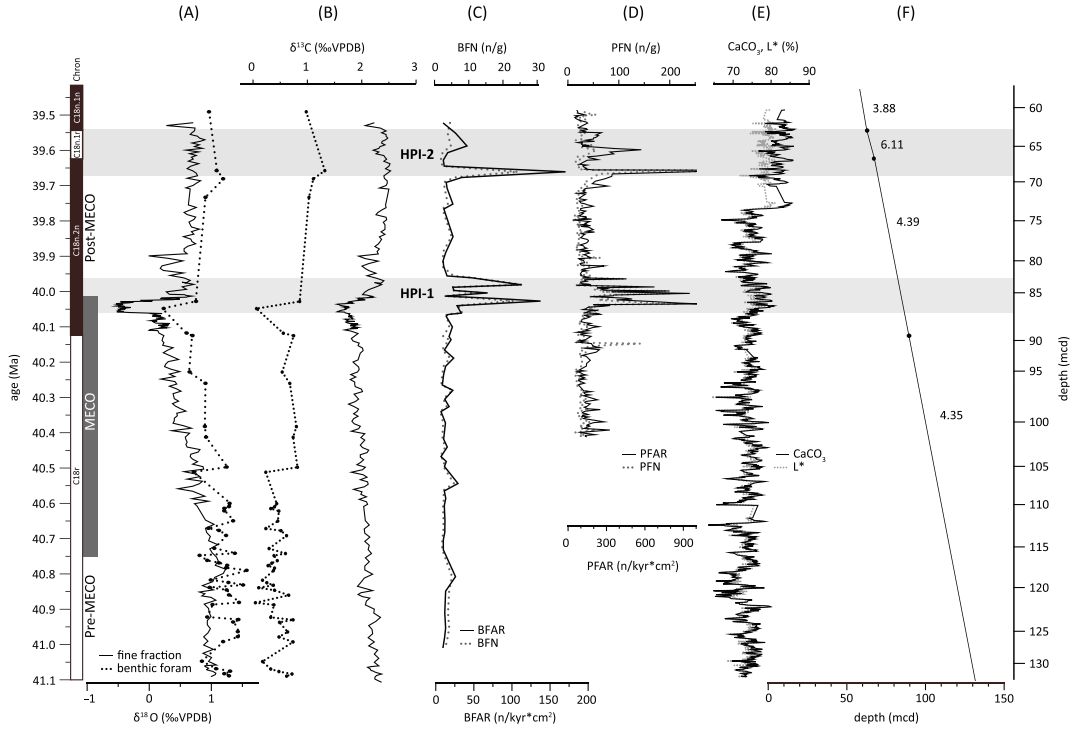

Figure 3. (a and b) Stable isotope records, (c and d) benthic and planktonic foraminiferal accumulation rates, (e) estimated weight % carbonate content, and (f) sedimentation rates from ODP Site 1051 across the MECO. Benthic and planktonic foraminiferal abundances (the solid lines are the accumulation rates, and the dotted lines are the absolute number of species/g) show two distinct peaks at ~40.0 Ma and ~39.7 Ma that are significantly higher than background values (highlighted in gray). $CaCO_3$ values (black line) were estimated from shipboard *L** values (gray line [*Norris et al.*, 1998]) and are consistently high throughout the section. Sedimentation rates are fairly constant except for a brief interval above HPI-2. Fine-fraction isotope data (solid line) are from *Bohaty et al.* [2009], and benthic foraminiferal isotope data (dotted line) are from *Edgar et al.* [2010].

L. sorachiensis, and *L. velascoensis*), *Nuttallides* spp. (mostly *N. truempyi*), *Osangularia mexicana*, *Pleurostomella* spp. (including *P. clavata*, *P. obtusa*, and *P. cubensis*), *Pullenia* spp. (*P. eocenia*, *P. angusta*, and *P. cretacea*), and *Strictocostella* spp.

The foraminiferal assemblages are typical of tropical Eocene environments and, notably, show only minor changes in species composition and/or abundance during the MECO (Figure 2). However, pronounced changes are evident in the accumulation rate of benthic and planktonic foraminifera during and after the MECO (Figures 3c and 3d). Benthic foraminiferal numbers and, accordingly, BFARs are generally very low (on average 23 n/cm^2/kyr) throughout the studied section, partially owing to dilution by abundant siliceous microfossils [*Edgar et al.*, 2010; *Norris et al.*, 1998; *Witkowski et al.*, 2014]. Planktonic foraminifera are more abundant, resulting in higher PFARs with an average of 100–150 n/cm^2/kyr. During two short-lived intervals between 40.07 to 39.96 Ma and 39.68 to 39.55 Ma, however, BFARs and PFARs both increase by about an order of magnitude to ~120 and ~1000 n/cm^2/kyr, respectively (shaded gray bars labeled "HPI-1" and "HPI-2" in Figure 3).

3.1. "Background" Conditions

In the following sections, background conditions (based on the BFAR and PFAR data here defined as encompassing the pre-MECO, the majority of the MECO, and parts of the post-MECO interval) will be discussed separately from the transient intervals characterized by elevated benthic and planktic foraminiferal accumulation rates.

Benthic foraminiferal assemblages show only minor variations in relative abundance prior to, and during, the majority of the MECO between 41.10 and 40.07 Ma (Figure 2). The most common taxa during this time interval (*Laevidentalina* spp., *Anomalinoides* spp., *Lenticulina* spp., *Pullenia* spp., and *Pleurostomella* spp.) are

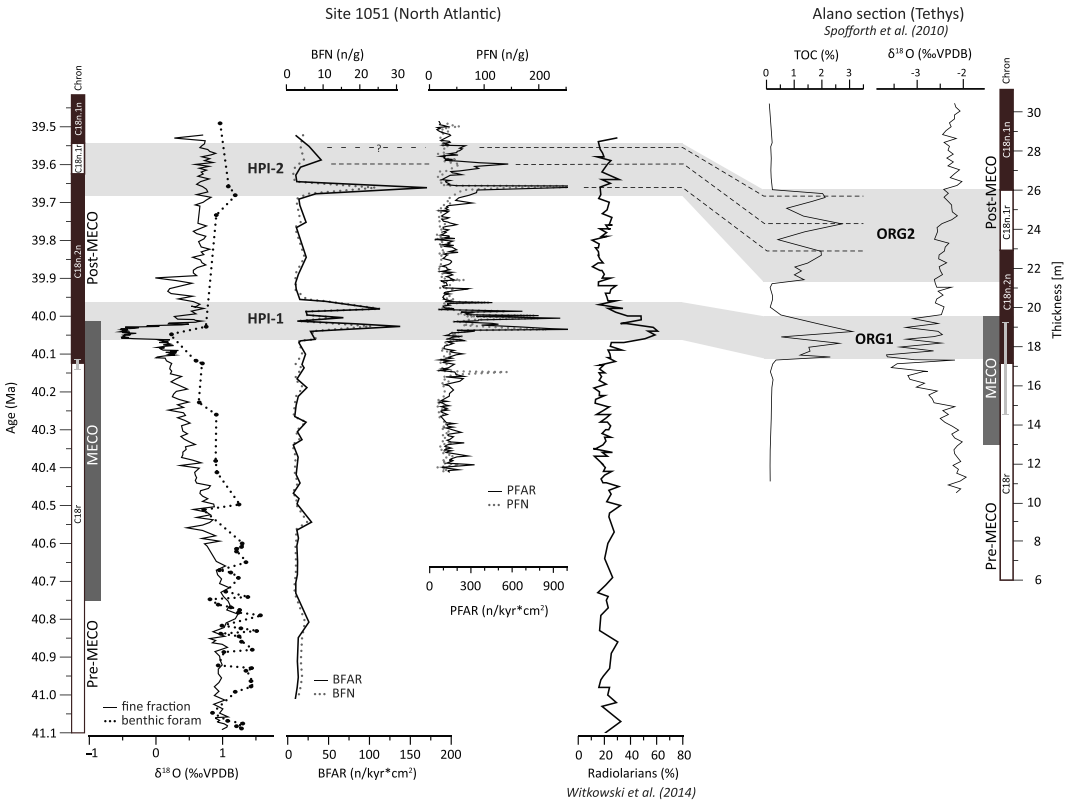

Figure 4. Comparison of our results from ODP Site 1051 with the relative abundance of radiolarians in the total siliceous microfossil assemblages [*Witkowski et al.*, 2014] from the same site. HPI-1 is reflected by an increase of radiolarians, suggesting a synchronous increase of primary and export production. HPI-1 and HPI-2 might be correlative with ORG1 and ORG2 [*Spofforth et al.*, 2010], indicating that productivity might have increased in several shelf locations. Differences in duration of the higher-productivity intervals are likely due to the comparison of different proxies and ocean basins and uncertainties of the placement of the chron C18r/18n.2n boundary. (The error bar is given in gray; for all other reversals, the error is too small to illustrate (>±1 cm).)

a mix of both infaunal und epifaunal species (Table 1). Average benthic foraminiferal numbers are low (<1 n/g) even for typically common deep-sea species, suggesting an environment which favored neither infaunal nor epifaunal taxa particularly.

Pleurostomellids decrease in abundance with decreasing benthic foraminiferal δ^{18}O values and inferred bottom water warming during the initial stages of the MECO (40.5 Ma) (Figure 2), suggesting that this genus was not well adapted to higher temperatures. At the same time, *Pullenia* spp. start to increase in abundance but subsequently decrease at ~40.28 Ma (Figure 2), perhaps indicating the presence of an environmental threshold. *Pullenia* spp. are infaunal taxa [*Corliss*, 1991; *Frenzel*, 1998] that are well adapted to eutrophic bottom water conditions [e.g., *Kaiho*, 1991; *Mackensen et al.*, 1993] but are typically found in cold water and used as an indicator for the influence of polar water masses [e.g., *Koch and Friedrich*, 2012; *Mackensen et al.*, 1993; *Widmark*, 1995]. Hence, we suggest that the abundance of *Pullenia* spp. initially increases due to increasing trophic state in bottom waters associated with the onset of the MECO warming but decreases once a certain temperature threshold is exceeded.

Crucially, the relatively muted benthic foraminiferal assemblage response and cooccurrence of both oligotrophic and eutrophic species (Table 1) imply that, taxonomically at least, benthic foraminifera were relatively insensitive to the environmental changes during the early stages of the MECO at ODP Site 1051. This is in stark contrast to the pronounced benthic foraminiferal response associated with the rapid onset of the PETM [e.g., *Thomas*, 1998; *Thomas and Shackleton*, 1996] and with a MECO section from the Southern Ocean [*Moebius et al.*, 2014] and may imply that the rate of environmental change during the MECO was gradual enough in the subtropical Atlantic Ocean to enable benthic foraminifera to adapt.

3.2. Higher-Productivity Intervals During and After the MECO

BFARs were initially developed as a proxy for export paleoproductivity by *Herguera and Berger* [1991] and have since been employed to estimate the amount of organic matter that is transported from surface waters to the ocean floor across a number of past climate intervals [e.g., *Den Dulk et al*., 2000; *Schmiedl et al*., 1997]. To semiquantify export production rates from BFARs it is required that several conditions are met. These include (1) a linear relationship between organic matter flux and number of fossilized foraminifera, (2) a linear relationship between surface water productivity and export productivity, (3) robust constraints on sedimentation rates, and (4) absence of carbonate dissolution [*Herguera and Berger*, 1991]. As mentioned previously, the sediments analyzed in this study show no obvious indications of dissolution implying that the drill site was situated well above the local CCD throughout the MECO [*Norris et al*., 1998]. The greatest source of uncertainty in our BFARs arises therefore from the assumption of constant linear sedimentation rates between magnetochrons because an orbital chronology is not yet available [*Edgar et al*., 2010]. The relationship between organic matter flux and fossilization, as well as that between surface and export productivity, is difficult to assess and requires some well-reasoned assumptions [*Herguera and Berger*, 1991]. Uncertainties in these parameters and a lack of reliable calibration have hindered the quantification of primary production in past environments [*Jorissen et al*., 2007]. However, it is possible to make qualitative predictions about relative changes in paleoproductivity from BFARs with high BFAR values typically reflecting enhanced food availability where confounding factors such as carbonate preservation are not an issue [e.g., *Coxall and Wilson*, 2011; *Jorissen et al*., 2007; *Van der Zwaan et al*., 1999].

In addition to the benthic foraminiferal abundances, we also investigate planktic foraminiferal accumulation rates (PFARs) that can also be interpreted in terms of productivity. The abundance of planktic foraminifera has been shown to exhibit a strong positive correlation with primary productivity [*Thunell and Reynolds*, 1984; *Van Kreveld*, 1997]. Thus, a number of studies have used this correlation to make quantitative assumptions about paleoproductivity based on planktic foraminiferal abundances, often in combination with BFARs and the accumulation rates of other marine organisms [e.g., *Boscolo Galazzo et al*., 2014; *Diester-Haass and Zahn*, 2001; *Hebbeln et al*., 2002; *Melki et al*., 2009; *Rasmussen et al*., 2003, 2014; *Van Kreveld*, 1997].

We identify two discrete intervals where BFARs and PFARs are an order of magnitude higher (>150 n/g) than background values (Figures 3c and 3d). Taken at face value, this suggests an increase in export productivity during the final stage of, and immediately following, the MECO at Site 1051. While we cannot quantify the assumed eutrophication, our data suggest that export productivity during these two transient intervals of elevated BFARs and PFARs was elevated compared to background conditions and that they are subsequently referred to as higher-productivity intervals (HPIs).

The first inferred higher-productivity interval (HPI-1) is ~110 kyr long and occurs between 40.07 and 39.96 Ma (Figures 3c and 3d). Its onset is synchronous with a significant decrease in δ^{18}O values corresponding to the rapid warming at the peak of the MECO and extends ~20 kyr after the MECO. At 40.02 Ma, BFARs briefly decrease (but, notably, still remain above background values) contemporaneous with the rapid increase in δ^{18}O and inferred ocean cooling marking the end of the MECO (Figure 3c). The abundances of most benthic taxa increase during HPI-1 (Figure 2), but the most pronounced increase occurs in *Strictocostella* spp. (5 n/g), *N. truempyi* (4 n/g), and most notably the opportunistic species *O. mexicana* (8 n/g). *Pyramidulina* spp. appear almost exclusively during HPI-1 (5 n/g), suggesting an opportunistic behavior, i.e., high tolerance to environmental changes and ability to adapt quickly. Other taxa that increase in abundance are *Laevidentalina* spp. (2 n/g), *O. umbonatus* (1.2 n/g), *Lenticulina* spp. (1.7 n/g), *Pleurostomella* spp. (0.8 n/g), and *Ellipsoidella* spp. (0.8 n/g; Figure 2). This comprises both epifaunal and infaunal species [e.g., *Alegret and Thomas*, 2001; *Frenzel*, 1998; *Friedrich and Hemleben*, 2007; *Friedrich et al*., 2003; *Kaiho*, 1999; *Mackensen et al*., 1993] (Table 1). The few taxa that either decrease in abundance or remain rare during HPI-1 are epifaunal (e.g., *Anomalinoides* spp. [*Alegret and Thomas*, 2004; *Takeda and Kaiho*, 2007]) and favor lower productivity environments. Taxa indicative of low-oxygen environments such as buliminids and uvigerinids [e.g., *Friedrich et al*., 2009; *Koutsoukos et al*., 1990] are either rare (<1%) or absent during HPI-1, suggesting that bottom waters on the Blake Nose Plateau were never significantly depleted in oxygen.

The second higher-productivity interval (HPI-2) occurs ~300 kyr later than HPI-1 (Figures 3c and 3d), ~100 kyr after the MECO (39.68–39.55 Ma), and lasts for ~130 kyr. The most pronounced increase in benthic

foraminiferal abundances during HPI-2 occurs in the taxa *N. truempyi*, *Laevidentalina* spp., *Siphonodosaria* spp., *O. umbonatus*, and *Lenticulina* spp.

Both HPIs are characterized by a substantial increase in the abundance of the majority of taxa, although the increase is generally more pronounced during HPI-1 compared to HPI-2 (Figure 2). There are some slight differences between the assemblages of both intervals: e.g., the much more pronounced increase of *Strictocostella* spp. and *O. mexicana* in HPI-1; the exclusive limitation of *Pyramidulina* spp. to HPI-1; and the higher abundance of *Siphonodosaria* spp., *Bulimina* spp., and *Lagena* spp. during HPI-2. Notably, both HPIs consist of several peaks within the events. This is especially well defined for HPI-2, where the BFARs show two and the planktonic foraminiferal numbers three distinct peaks that can be correlated between the two proxies. Yet the overall pattern of increasing BFAR and PFAR is similar during HPI-1 and HPI-2, and we thus suggest that similar environmental conditions prevailed.

Both HPIs occur within magnetrochrons and not at magnetochron boundaries (i.e., within each event, a single sedimentation rate was applied to calculate BFARs; see Figure 3). Hence, the observed peaks are unlikely to be mathematical artifacts arising from changes in sedimentation rate directly associated with our age model and more likely reflect a "real" signal. This observation is supported by the occurrence of synchronous peaks in the total benthic and planktonic foraminiferal numbers (Figures 3c and 3d) that are independent of the assumed linear sedimentation rates used to calculate accumulation rates.

It could be argued that these distinct increases in foraminiferal abundances might be the result of changing dilution by other particles or increased winnowing. Winnowing predominantly removes fine-fraction particles (such as diatoms and radiolarians) and thus leaves the sediments enriched in the bigger, heavier foraminifers. *Witkowski et al.* [2014] investigated siliceous microfossils (comprising the majority of the fine fraction) during the MECO at Site 1051. However, they do not detect minima in absolute siliceous microfossil abundances coinciding with maxima in foraminiferal abundances as would be expected if the sediments were subject to winnowing. On the contrary, they observe increases in all siliceous microfossil groups during the MECO, and radiolarians in particular show peak abundances coinciding with HPI-1 (Figure 4), also arguing against a significant decrease in dilution by nonforaminiferal components. Thus, we believe that neither winnowing nor changing dilution affected the investigated sediments to a significant degree and that our HPIs likely show ecologically driven changes.

3.3. Response of Benthic Foraminiferal Assemblages to Paleoceanographic Changes Related to MECO

The PETM and MECO are both major global warming events [e.g., *Bohaty and Zachos*, 2003; *Zachos et al.*, 2001, 2008]. Modern observations and numerical modeling predict that global ocean warming events will be accompanied by enhanced water column stratification, decreased oxygen saturation, and increases in surface water eutrophication in shelf and slope locations [*Keeling et al.*, 2010; *Plattner et al.*, 2001; *Sarmiento et al.*, 1998]. Therefore, oceanic warming associated with the MECO [e.g., *Bijl et al.*, 2010; *Bohaty and Zachos*, 2003; *Edgar et al.*, 2010] might, at first glance, be expected to impact benthic foraminiferal assemblages in a manner similar to that at the PETM. The PETM precipitated a global benthic foraminiferal extinction of ~25–65% of all taxa [*Thomas*, 1998] with ~55% of those at Site 1051 becoming extinct [*Katz et al.*, 1999] and is also associated with a large turnover from a highly diversified fauna to an assemblage dominated by infaunal taxa adapted to low-oxygen conditions (esp. bulimids [*Katz et al.*, 1999; *Takeda and Kaiho*, 2007]. Numerical modeling results point to a combination of deoxygenation of bottom waters, ocean acidification, and reduced food supply as probable explanations for the observed benthic extinctions [*Winguth et al.*, 2012]. In contrast to this expectation, benthic foraminiferal assemblages show almost no change associated with the MECO (Figure 2), except for the two HPIs between 40.07–39.98 Ma and 39.68–39.55 Ma, here inferred to represent an increase in organic matter flux to the seafloor.

Possible explanations for this seeming contradiction are that environmental changes at this site were subdued or much more gradual compared to other locations.

First, potential changes in bottom water trophic state and oxygenation associated with the MECO were minor at this site. Despite the inferred rise in oceanic temperatures at Site 1051 based on $\delta^{18}O$ [*Bohaty et al.*, 2009; *Edgar et al.*, 2010], the water column at the site might have remained well ventilated across the MECO and was thus not subject to enhanced stratification and consequential bottom water oxygen depletion. The cooccurrence of both infaunal and epifaunal species throughout the study interval further implies a more

Table 2. Summary of All Publications on the MECO Interval, Sorted by Ocean Basin[a]

Site	Inferred Changes in Trophic State	Proxy
	Tethys	
Alano section	Surface and bottom water productivity elevated at peak warming and afterward [*Luciani et al.*, 2010; *Spofforth et al.*, 2010]	% total organic carbon planktic foraminifera assemblages
	Bottom water productivity elevated during peak warming and post-MECO [*Boscolo Galazzo et al.*, 2013]	Benthic foraminifera assemblages
Contessa section	No data [*Jovane et al.*, 2007]	
	North Atlantic	
ODP Site 1051	Bottom water productivity elevated at peak warming and later (this study)	Benthic foraminiferal accumulation rates
	Surface water productivity elevated during the MECO and onset of peak warming [*Witkowski et al.*, 2014]	Siliceous microfossil accumulation rates
	South Atlantic	
ODP Site 1260A	Surface water productivity elevated during the MECO [*Renaudie et al.*, 2010]	Siliceous phytoplankton assemblages and accumulation rates
	Possible decline in export productivity [*Sexton et al.*, 2006]	$\Delta\delta^{13}C$
ODP Site 1263	Elevated export productivity during the early MECO, decline during peak warming [*Boscolo Galazzo et al.*, 2014, 2015]	Benthic foraminifera assemblages and benthic foraminiferal accumulation rates
DSDP Site 523	No data [*Bohaty et al.*, 2009]	
ODP Site 702	No data [*Bohaty et al.*, 2009]	
	Southern Ocean	
ODP Sites 748 and 749	Surface water productivity elevated during MECO warming [*Witkowski et al.*, 2012]	Siliceous microfossil accumulation rates
ODP Site 738	Bottom water productivity elevated during MECO warming (Moebius et al., submitted)	Benthic foraminifera assemblages
ODP Site 689	No data [*Bohaty and Zachos*, 2003; *Bohaty et al.*, 2009]	
ODP Sites 1172 and 1171	No data [*Bijl et al.*, 2009, 2010, 2011]	
	Pacific Ocean	
IODP Site U1331	No data [*Kamikuri et al.*, 2013]	
ODP Sites 1218 and 1219	No data [*Lyle et al.*, 2005]	
ODP Site 1209	No data [*Dawber and Tripati*, 2011]	
	Indian Ocean	
ODP Site 709	No data [*Peterson et al.*, 1990]	
ODP Site 711	No data [*Peterson et al.*, 1990]	

[a]Column 1 indicates the site described in the publication, column 2 summarizes the authors assumptions about changes in trophic state, and column 3 lists the proxy used for their interpretations. Increases in trophic state are observed in many shelf/slope locations, but the timing and duration vary within different proxies and ocean basins.

or less consistently mesotrophic environment [*Jorissen*, 2003]. However, this explanation is in contrast to the observed increases in BFARs and PFARs in the latest phase of the MECO, indicating some increase in bioproductivity.

Second, any potential changes in eutrophication and oxygenation might have been much more gradual during the MECO than experienced during the PETM and thus have allowed taxa to adapt to environmental change. The onset of the PETM likely occurred in >10 kyr [e.g., *Sluijs et al.*, 2012; *Thomas*, 2003; *Thomas and Shackleton*, 1996], whereas the warming during the MECO took place over a much longer interval of time (~600 kyr) and thus may have occurred at a pace sufficiently gradual enough to allow benthic ecosystems to slowly adjust. The onset of the peak warming on the other hand (coinciding with HPI-1) was an abrupt 50 kyr long interval of greatly accelerated temperature increase at ~40 Ma (Figure 3a). This coincidence tentatively implies that the rapidity of the warming within this interval was responsible for the observed faunal reaction, because the speed of change limited the ability of certain foraminifera to adapt. Alternatively, the crossing of an ecological tolerance threshold may have precipitated the ecological changes associated with HPI-1. In contrast, a site on the Kerguelen Plateau was

subject to a significant faunal turnover during the more gradual warming phase of the MECO [*Moebius et al.*, 2014], arguing against the possibility of gradual adaptation of taxa in the Southern Ocean.

Consequently, we assume that other, site-specific factors, such as the type of food delivered to the seafloor, might have had an impact on benthic foraminiferal assemblages and abundances. However, such dependencies are not well defined in the paleontological record thus far.

Nevertheless, assuming that the changes in foraminiferal abundance reflect a true ecological signal, their pronounced increases during HPI-1 and HPI-2 point toward increasing organic matter flux during these intervals.

3.4. Potential Scenarios for a Local Increase in Organic Matter Flux

At Site 1051, several possible mechanisms exist to explain the inferred increase in export productivity: (1) a change in ocean circulation, (2) upwelling of nutrient-rich waters, and/or (3) increasing continental runoff.

The first mechanism, a significant shift in the bottom water mass bathing ODP Site 1051, is unlikely, because of the lack of change in the benthic foraminiferal assemblage composition (Figure 2). The second mechanism, upwelling of nutrient-rich waters, commonly gives rise to high surface productivity. Although the western margin of the Atlantic Ocean is not an upwelling locality at present, several studies have suggested that the Blake Plateau may have been the locus of Ekman upwelling during the Eocene [*Wade et al.*, 2001] and Late Cretaceous [*MacLeod et al.*, 2001]. Thus, shifts in the location of upwelling or an increase in upwelling intensity due to changes in the coastal wind system (intensification or change of direction) could have lead to transient changes in local productivity. The third mechanism, intensified continental runoff (and the nutrients that it delivers), would strengthen biological productivity at locations close to the continental margin such as Blake Plateau [cf. *MacLeod et al.*, 2001]. Climatic warming, such as the MECO peak warming, is likely to be associated with an intensified hydrological cycle [e.g., *Montero-Serrano et al.*, 2011; *Norris et al.*, 2013; *Nürnberg et al.*, 2008], leading to an increase in riverine input into the ocean. Certainly, there are multiple lines of evidence for an increase in terrestrial runoff to the ocean during the MECO at marginal sites in the Tethyan Ocean [*Agnini et al.*, 2007; *Luciani et al.*, 2010; *Spofforth et al.*, 2010; *Toffanin et al.*, 2011]. Further, siliceous microfossil assemblages from ODP Site 1051 also indicate an overall increase in the trophic state of surface waters and infer increased delivery of silica from elevated silicate weathering across the MECO [*Witkowski et al.*, 2014].

However, our benthic and planktic foraminiferal assemblage data alone do not allow us to distinguish between upwelling and/or runoff-driven hypotheses to explain the increase in productivity at ODP Site 1051. At relatively nearshore sites, an increased input of siliciclastic material would be expected to be associated with continental runoff and riverine input. Evidence for such siliciclastic input at Site 1051 is absent, but the distance of 500 km to the shore was likely too far for transport of significant amounts of terrestrial material to the site, as it would more likely become trapped on the continental shelf. Nutrients, on the other hand, are more likely to reach a location ~500 km offshore in suspension to intensify surface and export productivity. Accounting for these uncertainties, however, we compare our results with those from nearshore sites in other settings to ascertain whether the change in productivity is a local signal of Site 1051 or if there is evidence for a more global signal.

3.5. Global Increase in Trophic State Associated With the MECO

Figure 4 shows that the abundance of siliceous radiolarians (another group of zooplankton) increased threefold at Site 1051, concurrent with our HPI-1 event [*Witkowski et al.*, 2014]. Our HPIs also appear to coincide with organic-rich layers (ORG1 and ORG2) identified in the Alano section in northern Italy [*Luciani et al.*, 2010; *Spofforth et al.*, 2010]. The ORG layers at Alano are defined by significant increases in TOC (2.5–3.0%) relative to background values (0.1%) and are coincident with elevated $\delta^{13}C$ values [*Spofforth et al.*, 2010] that are accompanied by oxygen depletion in the water column as evidenced by calcareous nannofossil and planktic foraminiferal assemblages [*Jovane et al.*, 2007; *Luciani et al.*, 2010]. Specifically, a pronounced increase in the relative abundance of the cool, eutrophic water favoring planktonic foraminifera *Subbotina*, which in the absence of evidence for cooling during the MECO likely reflects an increase in the availability of nutrients in surface waters [*Luciani et al.*, 2010], is in agreement with increasing numbers of siliceous microfossils [*Toffanin et al.*, 2011]. Increases in surface and export productivity have been invoked to explain these organic-rich intervals at this site [*Spofforth et al.*, 2010].

To correlate records from the two sites we used the available site-specific magnetostratigraphies [*Agnini et al*., 2011; *Edgar et al*., 2010]. Figure 4 shows that at Alano, given the uncertainty in the magnostratigraphy, ORG1 commences somewhere near the base of chron C18n.2n and persists into the first third of C18n.2n, while ORG2 initiates in the upper third of C18n.2n and spans most of C18n.1r [*Spofforth et al*., 2010]. This occurrence of the ORG layers in Alano is, within the uncertainties of both age models, in relatively close agreement with our HPIs from Site 1051 (Figure 4). We note, however, that the HPIs at Site 1051 are of slightly shorter duration relative to magnetochron duration than the ORGs at Alano (Figure 4). However, the relatively poorly constrained placement of the base of C18n.2n in the Alano section (±4.85 m) [*Spofforth et al*., 2010] most likely contributes to the slightly different appearance of the events. It should also be noted that C18n.1r is artificially enhanced in apparent duration at Alano (Figure 4) because these particular data are plotted against depth rather than age (because no sufficiently good age model exists for Alano). It is also possible that the two different proxies (TOC versus BFAR) record subtly different environmental variables that were perturbed to different extents. Nonetheless, ORG2 exhibits three distinct peaks similar to the PFAR record from our site (only two peaks in the BFARs, possibly due to sample resolution). This apparent correlation (dashed lines in Figure 4) further strengthens our interpretation of the likely coinciding occurrence of HPI-2 and ORG2.

Eutrophication events associated with the MECO were also observed in several other locations. Increased productivity is found in benthic foraminiferal assemblage composition data [*Moebius et al*., 2014] and siliceous microfossil assemblage composition and abundance data [*Witkowski et al*., 2012] in the Southern Ocean (Kerguelen Plateau). At Demerara Rise in the western South Atlantic, *Renaudie et al.* [2010] found evidence for an increase in surface water eutrophication based on siliceous microfossil abundances during the MECO at Site 1260. However, the post-MECO interval is not represented in this section, hindering further correlation with this data set. New records from Walvis Ridge in the eastern South Atlantic (Site 1263) also show evidence for increased productivity associated with the MECO [*Boscolo Galazzo et al*., 2014, 2015]. Although the composition of benthic foraminiferal assemblages was not significantly affected by the environmental changes during the MECO, benthic and planktic foraminiferal abundances both increase during the MECO at Site 1263 [*Boscolo Galazzo et al*., 2015], similar to our results at Site 1051. However, peaks in foraminiferal accumulation rates at Site 1263 precede the peak-warming interval (and HPI-1) by several thousand years, which is attributed to foraminiferal starvation due to increases in the metabolic rates at this site in response to warming [*Boscolo Galazzo et al*., 2014].

The occurrence of intervals of apparent eutrophication in widely separated different geographic settings and ocean basins (e.g., contrasting latitudes, proximal, and distal to adjacent continents and in the Southern Ocean, Tethys, and the Atlantic Oceans; see Table 2) suggests that an increase in productivity may have been globally widespread across the MECO, akin to the widespread eutrophication experience during the PETM [*Gibbs et al*., 2006; *Norris et al*., 2013; *Winguth et al*., 2012]. The extent and duration of eutrophication and its effect on the benthic and planktonic communities, however, appear to differ between locations (Figure 1 in *Boscolo Galazzo et al.* [2015]). At subtropical Site 1051 and in the Tethyan Alano section, the increase in trophic state seems to be restricted to the peak-warming interval, while eutrophication begins much earlier at 40.4 Ma (300 kyr before peak warming) in the Southern Ocean and southern Atlantic. The response of the benthic foraminiferal communities ranges from very strong at Site 738 (in form of a faunal turnover) [*Moebius et al*., 2014], to apparent but less pronounced in the Tethys [*Boscolo Galazzo et al*., 2013], to muted at Site 1051 (this study) and Site 1263 (South Atlantic) [*Boscolo Galazzo et al*., 2014, 2015]. Furthermore, it appears that different microfossil groups (benthic and planktonic foraminifera, diatoms, radiolarians) reacted differently to a similar environmental perturbation, which might be attributed to the specific local environmental conditions at each site.

While localized changes in the position or intensity of upwelling are unlikely to have been the mechanism for increased eutrophication in many ocean basins, an intensification of the hydrological cycle under extreme greenhouse warming during the MECO [*Bohaty et al*., 2009] might have acted as the driver of a widespread increase in surface water productivity via enhanced nutrient availability and subsequent strengthened export production to the seafloor.

4. Conclusion

We present benthic foraminiferal assemblage data alongside benthic and planktonic abundances from ODP Site 1051 in the subtropical North Atlantic, spanning the MECO and post-MECO intervals. We observe two

intervals (higher-productivity intervals HPI-1 and HPI-2) during peak warming and ~300 kyr following the MECO that are marked by benthic and planktonic foraminiferal accumulation rates that increase by an order of magnitude. These HPIs are paralleled by increasing radiolarian abundances at Site 1051. We conclude that these intervals represent periods of enhanced biological productivity, potentially driven by a strengthened hydrological cycle. We note that higher-productivity intervals associated with the MECO are reported from many, widely distributed marginal-marine locations, including the Alano section (paleo-Tethys seaway), the Kerguelen Plateau (Southern Ocean), and Walvis Ridge (South Atlantic), with the impact on benthic foraminiferal community composition being most pronounced in the Southern Ocean. We thus suggest that marine continental shelf and slope settings may have witnessed increased eutrophication across the MECO, resulting in one or more episodes of intensified biological (export) productivity.

Acknowledgments

All data generated in this study are available in Data Sets S1 and S2 in the supporting information. We are grateful to Paul A. Wilson (National Oceanography Centre Southampton, UK) and Richard D. Norris (Scripps Institution of Oceanography, La Jolla, USA) who provided assistance with processing the samples used in this study. Three anonymous reviewers, Appy Sluijs, and the Editor (Christopher Charles) provided helpful comments and suggestions to improve the manuscript. The Integrated Ocean Drilling Program (IODP) provided the samples used in this study. The IODP is sponsored by the U.S. National Science Foundation and participating countries under the management of Joint Oceanographic Institutions, Inc. Funding for this study was provided by the German Research Foundation (DFG) to O.F. (Emmy-Noether research group "Meso- and Cenozoic Paleoceanography," grant FR 2544/2-1), a Natural Environment Research Council Postdoctoral Research Fellowship (NE/H016457/1) and Leverhulme Early Career Fellowship (ECF-2013-608) to K.M.E., a European Commission Marie Curie Outgoing International Fellowship to P.F.S., and a Leverhulme Trust Fellowship to P.F.S.

References

Agnini, C., D. Spofforth, E. Fornaciari, L. Giusberti, L. Lanci, V. Luciani, G. Muttoni, H. Pälike, and D. Rio (2007), Is the Middle Eocene Climatic Optimum (MECO) recorded in the central-western Tethys?, Abstract OS11A-0188 presented at 2007 Fall Meeting, AGU.

Agnini, C., E. Fornaciari, L. Giusberti, P. Grandesso, L. Lanci, V. Luciani, G. Muttoni, H. Pälike, D. Rio, and D. J. Spofforth (2011), Integrated biomagnetostratigraphy of the Alano section (NE Italy): A proposal for defining the middle-late Eocene boundary, *Geol. Soc. Am. Bull.*, *123*(5–6), 841–872.

Alegret, L., and E. Thomas (2001), Upper Cretaceous and lower Paleogene benthic foraminifera from northeastern Mexico, *Micropaleontology*, *47*(4), 269–316.

Alegret, L., and E. Thomas (2004), Benthic foraminifera and environmental turnover across the Cretaceous/Paleogene boundary at Blake Nose (ODP Hole 1049C, northwestern Atlantic), *Palaeogeogr. Palaeoclimatol. Palaeoecol.*, *208*(1), 59–83.

Alegret, L., and E. Thomas (2005), Cretaceous/Paleogene boundary bathyal paleo-environments in the central North Pacific (DSDP Site 465), the northwestern Atlantic (ODP Site 1049), the Gulf of Mexico and the Tethys: The benthic foraminiferal record, *Palaeogeogr. Palaeoclimatol. Palaeoecol.*, *224*(1), 53–82.

Alegret, L., S. Ortiz, X. Orue-Etxebarria, G. Bernaola, J. I. Baceta, S. Monechi, E. Apellaniz, and V. Pujalte (2009), The Paleocene-Eocene Thermal Maximum: New data on microfossil turnover at the Zumaia section, Spain, *Palaios*, *24*(5), 318–328.

Badawi, A., G. Schmiedl, and C. Hemleben (2005), Impact of late Quaternary environmental changes on deep-sea benthic foraminiferal faunas of the Red Sea, *Mar. Micropaleontol.*, *58*(1), 13–30.

Bhaumik, A. K., A. K. Gupta, and E. Thomas (2011), Blake Outer Ridge: Late Neogene variability in paleoceanography and deep-sea biota, *Palaeogeogr. Palaeoclimatol. Palaeoecol.*, *302*(3-4), 435–451.

Bijl, P. K., S. Schouten, A. Sluijs, G.-J. Reichart, J. C. Zachos, and H. Brinkhuis (2009), Early Palaeogene temperature evolution of the southwest Pacific Ocean, *Nature*, *461*(7265), 776–779.

Bijl, P. K., A. J. P. Houben, S. Schouten, S. M. Bohaty, A. Sluijs, G.-J. Reichart, J. S. Sinninghe Damsté, and H. Brinkhuis (2010), Transient middle Eocene atmospheric CO_2 and temperature variations, *Science*, *330*(6005), 819–821.

Bijl, P. K., J. Pross, J. Warnaar, C. E. Stickley, M. Huber, R. Guerstein, A. J. P. Houben, A. Sluijs, H. Visscher, and H. Brinkhuis (2011), Environmental forcings of Paleogene Southern Ocean dinoflagellate biogeography, *Paleoceanography*, *26*, PA1202, doi:10.1029/2009PA001905.

Bohaty, S. M., and J. C. Zachos (2003), Significant Southern Ocean warming event in the late middle Eocene, *Geology*, *31*(11), 1017.

Bohaty, S. M., J. C. Zachos, F. Florindo, and M. L. Delaney (2009), Coupled greenhouse warming and deep-sea acidification in the middle Eocene, *Paleoceanography*, *24*, PA2207, doi:10.1029/2008PA001676.

Bolli, H. M., J. P. Beckmann, and J. B. Saunders (1994), *Benthic Foraminiferal Biostratigraphy of the South Caribbean Region*, 408 pp., Cambridge Univ. Press, Cambridge, U. K.

Boscolo Galazzo, F., L. Giusberti, V. Luciani, and E. Thomas (2013), Paleoenvironmental changes during the Middle Eocene Climatic Optimum (MECO) and its aftermath: The benthic foraminiferal record from the Alano section (NE Italy), *Palaeogeogr. Palaeoclimatol. Palaeoecol.*, *378*, 22–35.

Boscolo Galazzo, F., E. Thomas, M. Pagani, C. Warren, V. Luciani, and L. Giusberti (2014), The Middle Eocene Climatic Optimum (MECO): A multiproxy record of paleoceanographic changes in the southeast Atlantic (ODP Site 1263, Walvis Ridge), *Paleoceanography*, *29*, 1143–1161, doi:10.1002/2014PA002670.

Boscolo Galazzo, F., E. Thomas, and L. Giusberti (2015), Benthic foraminiferal response to the Middle Eocene Climatic Optimum (MECO) in the South-Eastern Atlantic (ODP Site 1263), *Palaeogeogr. Palaeoclimatol. Palaeoecol.*, *417*, 432–444.

Burgess, C. E., P. N. Pearson, C. H. Lear, H. E. G. Morgans, L. Handley, R. D. Pancost, and S. Schouten (2008), Middle Eocene climate cyclicity in the southern Pacific: Implications for global ice volume, *Geology*, *36*(8), 651–654.

Cande, S. C., and D. V. Kent (1995), Revised calibration of the geomagnetic polarity timescale for the Late Cretaceous and Cenozoic, *J. Geophys. Res.*, *100*(B4), 6093–6095, doi:10.1029/94JB03098.

Coccioni, R., and S. Galeotti (1993), Orbitally induced cycles in benthonic foraminiferal morphogroups and trophic structure distribution patterns from the Late Albian "Amadeus Segment" (central Italy), *J. Micropalaeontol.*, *12*(2), 227–239.

Corliss, B. H. (1991), Morphology and microhabitat preferences of benthic foraminifera from the northwest Atlantic Ocean, *Mar. Micropaleontol.*, *17*(3), 195–236.

Corliss, B. H., and C. Chen (1988), Morphotype patterns of Norwegian Sea deep-sea benthic foraminifera and ecological implications, *Geology*, *16*(8), 716–719.

Coxall, H. K., and P. A. Wilson (2011), Early Oligocene glaciation and productivity in the eastern equatorial Pacific: Insights into global carbon cycling, *Paleoceanography*, *26*, PA2221, doi:10.1029/2010PA002021.

Coxall, H. K., P. A. Wilson, H. Pälike, C. H. Lear, and J. Backman (2005), Rapid stepwise onset of Antarctic glaciation and deeper calcite compensation in the Pacific Ocean, *Nature*, *433*(7021), 53–57.

Cramer, B., J. Toggweiler, J. Wright, M. Katz, and K. Miller (2009), Ocean overturning since the Late Cretaceous: Inferences from a new benthic foraminiferal isotope compilation, *Paleoceanography*, *24*, PA4216, doi:10.1029/2008PA001683.

Dawber, C. F., and A. K. Tripati (2011), Constraints on glaciation in the middle Eocene (46–37 Ma) from Ocean Drilling Program (ODP) Site 1209 in the tropical Pacific Ocean, *Paleoceanography*, *26*, PA2208, doi:10.1029/2010PA002037.

DeConto, R. M., S. Galeotti, M. Pagani, D. Tracy, K. Schaefer, T. Zhang, D. Pollard, and D. J. Beerling (2012), Past extreme warming events linked to massive carbon release from thawing permafrost, *Nature*, *484*(7392), 87–91.
Den Dulk, M., G. J. Reichart, S. Van Heyst, W. Zachariasse, and G. Van der Zwaan (2000), Benthic foraminifera as proxies of organic matter flux and bottom water oxygenation? A case history from the northern Arabian Sea, *Palaeogeogr. Palaeoclimatol. Palaeoecol.*, *161*(3), 337–359.
Dickens, G. R., J. R. O'Neil, D. K. Rea, and R. M. Owen (1995), Dissociation of oceanic methane hydrate as a cause of the carbon isotope excursion at the end of the Paleocene, *Paleoceanography*, *10*(6), 965–971, doi:10.1029/95PA02087.
Diester-Haass, L., and R. Zahn (2001), Paleoproductivity increase at the Eocene-Oligocene climatic transition: ODP/DSDP Sites 763 and 592, *Palaeogeogr. Palaeoclimatol. Palaeoecol.*, *172*(1), 153–170.
Drinia, H., N. Tsaparas, A. Antonarakou, and G. Goumas (2003), Benthic foraminiferal biofacies associated with middle to early late Miocene oxygen deficient conditions in the eastern Mediterranean, paper presented at International Conference on Environmental Science and Technology, Lemnos Island, Greece, 8–10 Sept.
Edgar, K., P. Wilson, P. Sexton, S. Gibbs, A. Roberts, and R. Norris (2010), New biostratigraphic, magnetostratigraphic and isotopic insights into the Middle Eocene Climatic Optimum in low latitudes, *Palaeogeogr. Palaeoclimatol. Palaeoecol.*, *297*, 670–682.
Edgar, K., S. Bohaty, S. Gibbs, P. Sexton, R. Norris, and P. Wilson (2013), Symbiont "bleaching" in planktic foraminifera during the Middle Eocene Climatic Optimum, *Geology*, *41*(1), 15–18.
Edgar, K. M., P. A. Wilson, P. F. Sexton, and Y. Suganuma (2007), No extreme bipolar glaciation during the main Eocene calcite compensation shift, *Nature*, *448*(7156), 908–911.
Eldholm, O., and E. Thomas (1993), Environmental impact of volcanic margin formation, *Earth Planet. Sci. Lett.*, *117*(3), 319–329.
Erbacher, J., W. Gerth, G. Schmiedl, and C. Hemleben (1998), Benthic foraminiferal assemblages of late Aptian-early Albian black shale intervals in the Vocontian Basin, SE France, *Cretaceous Res.*, *19*(6), 805–826.
Erbacher, J., C. Hemleben, B. T. Huber, and M. Markey (1999), Correlating environmental changes during early Albian oceanic anoxic event 1B using benthic foraminiferal paleoecology, *Mar. Micropaleontol.*, *38*(1), 7–28.
Fassell, M. L., and T. J. Bralower (1999), Warm, equable mid-Cretaceous: Stable isotope evidence, in *Evolution of the Cretaceous Ocean-Climate System*, edited by E. Barrera and C. C. Johnson, pp. 121–142, Geol. Soc. Am, Spec. Pap., Boulder, Colo.
Frenzel, P. (1998), Die benthischen Foraminiferen der Rügener Schreibkreide (Unter-Maastrichtium, NE-Deutschland), PhD thesis, 327 pp., Univ. of Greifswald.
Friedrich, O. (2010), Benthic foraminifera and their role to decipher paleoenvironment during mid-Cretaceous oceanic anoxic events: The "anoxic benthic foraminifera" paradox, *Rev. Micropaleontol.*, *53*(3), 175–192.
Friedrich, O., and J. Erbacher (2006), Benthic foraminiferal assemblages from Demerara Rise (ODP Leg 207, western tropical Atlantic): Possible evidence for a progressive opening of the equatorial Atlantic gateway, *Cretaceous Res.*, *27*(3), 377–397.
Friedrich, O., and C. Hemleben (2007), Early Maastrichtian benthic foraminiferal assemblages from the western North Atlantic (Blake Nose) and their relation to paleoenvironmental changes, *Mar. Micropaleontol.*, *62*(1), 31–44.
Friedrich, O., K. Reichelt, J. O. Herrle, J. Lehmann, J. Pross, and C. Hemleben (2003), Formation of the Late Aptian Niveau Fallot black shales in the Vocontian Basin (SE France): Evidence from foraminifera, palynomorphs, and stable isotopes, *Mar. Micropaleontol.*, *49*(1), 65–85.
Friedrich, O., H. Nishi, J. Pross, G. Schmiedl, and C. Hemleben (2005), Millennial-to centennial-scale interruptions of the oceanic anoxic event 1b (Early Albian, mid-Cretaceous) inferred from benthic foraminiferal repopulation events, *Palaios*, *20*(1), 64–77.
Friedrich, O., G. Schmiedl, and H. Erlenkeuser (2006), Stable isotope composition of Late Cretaceous benthic foraminifera from the southern South Atlantic: Biological and environmental effects, *Mar. Micropaleontol.*, *58*(2), 135–157.
Friedrich, O., J. O. Herrle, P. A. Wilson, M. J. Cooper, J. Erbacher, and C. Hemleben (2009), Early Maastrichtian carbon cycle perturbation and cooling event: Implications from the South Atlantic Ocean, *Paleoceanography*, *24*, PA2211, doi:10.1029/2008PA001654.
Gibbs, S. J., T. J. Bralower, P. R. Bown, J. C. Zachos, and L. M. Bybell (2006), Shelf and open-ocean calcareous phytoplankton assemblages across the Paleocene-Eocene Thermal Maximum: Implications for global productivity gradients, *Geology*, *34*(4), 233–236.
Gooday, A. J. (1994), The biology of deep-sea foraminifera: A review of some advances and their applications in paleoceanography, *Palaios*, *9*, 14–31.
Gooday, A. J. (2003), Benthic foraminifera (Protista) as tools in deep-water palaeoceanography: Environmental influences on faunal characteristics, *Adv. Mar. Biol.*, *46*, 1–90.
Hay, W. W., et al. (1999), Alternative global cretaceous paleogeography, in Evolution of the Cretaceous Ocean-Climate System, edited by E. Barrera and C. C. Johnson, p. 1, Geol. Soc. of Am. Spec. Pap., Boulder, Colo.
Hebbeln, D., M. Marchant, and G. Wefer (2002), Paleoproductivity in the southern Peru-Chile Current through the last 33,000 yr, *Mar. Geol.*, *186*(3), 487–504.
Herguera, J. C., and W. Berger (1991), Paleoproductivity from benthic foraminifera abundance: Glacial to postglacial change in the west-equatorial Pacific, *Geology*, *19*(12), 1173–1176.
Higgins, J. A., and D. P. Schrag (2006), Beyond methane: Towards a theory for the Paleocene-Eocene Thermal Maximum, *Earth Planet. Sci. Lett.*, *245*(3), 523–537.
Hollis, C. J., et al. (2009), Tropical sea temperatures in the high-latitude South Pacific during the Eocene, *Geology*, *37*(2), 99–102.
Jorissen, F. J. (2003), Benthic foraminiferal microhabitats below the sediment-water interface, in *Modern Foraminifera*, edited by B. K. S. Gupta, pp. 161–179, Kluwer Acad., Dordrecht, Netherlands.
Jorissen, F. J., H. C. de Stigter, and J. G. Widmark (1995), A conceptual model explaining benthic foraminiferal microhabitats, *Mar. Micropaleontol.*, *26*(1), 3–15.
Jorissen, F. J., C. Fontanier, and E. Thomas (2007), Paleoceanographical proxies based on deep-sea benthic foraminiferal assemblage characteristics, in *Proxies in Late Cenozoic Paleoceanography: Part 2: Biological Tracers and Biomarkers*, edited by C. Hillaire-Marcel and A. de Vernal, pp. 263–326, Elsevier, Amsterdam.
Jovane, L., F. Florindo, R. Coccioni, J. Dinarès-Turell, A. Marsili, S. Monechi, A. P. Roberts, and M. Sprovieri (2007), The Middle Eocene Climatic Optimum event in the Contessa Highway section, Umbrian Apennines, Italy, *Geol. Soc. Am. Bull.*, *119*(3-4), 413.
Kaiho, K. (1991), Global changes of Paleogene aerobic/anaerobic benthic foraminifera and deep-sea circulation, *Palaeogeogr. Palaeoclimatol. Palaeoecol.*, *83*(1-3), 65–85.
Kaiho, K. (1992a), Eocene to Quaternary benthic foraminifers and paleobathymetry of the Izu-Bonin arc, Legs 125 and 126, *Proc. Ocean Drill. Program Sci. Results*, *126*, 285–310.
Kaiho, K. (1992b), A low extinction rate of intermediate-water benthic foraminifera at the Cretaceous/Tertiary boundary, *Mar. Micropaleontol.*, *18*(3), 229–259.
Kaiho, K. (1999), Effect of organic carbon flux and dissolved oxygen on the benthic foraminiferal oxygen index (BFOI), *Mar. Micropaleontol.*, *37*(1), 67–76.

Kaiho, K., and T. Hasegawa (1994), End-Cenomanian benthic foraminiferal extinctions and oceanic dysoxic events in the northwestern Pacific Ocean, *Palaeogeogr. Palaeoclimatol. Palaeoecol.*, *111*(1), 29–43.
Kamikuri, S.-i., T. C. Moore, M. Lyle, K. Ogane, and N. Suzuki (2013), Early and Middle Eocene radiolarian assemblages in the eastern equatorial Pacific Ocean (IODP Leg 320 Site U1331): Faunal changes and implications for paleoceanography, *Mar. Micropaleontol.*, *98*(0), 1–13.
Katz, M. E., D. K. Pak, G. R. Dickens, and K. G. Miller (1999), The source and fate of massive carbon input during the latest Paleocene Thermal Maximum, *Science*, *286*(5444), 1531–1533.
Keeling, R. F., A. Körtzinger, and N. Gruber (2010), Ocean deoxygenation in a warming world, *Annu. Rev. Mar. Sci.*, *2*, 199–229.
Kennett, J. P., and L. Stott (1991), Abrupt deep-sea warming, palaeoceanographic changes and benthic extinctions at the end of the Palaeocene, *Nature*, *353*, 225–229.
Koch, M. C., and O. Friedrich (2012), Campanian-Maastrichtian intermediate- to deep-water changes in the high latitudes: Benthic foraminiferal evidence, *Paleoceanography*, *27*, PA2209, doi:10.1029/2011PA002259.
Koutsoukos, E. A., and M. B. Hart (1990), Cretaceous foraminiferal morphogroup distribution patterns, palaeocommunities and trophic structures: A case study from the Sergipe Basin, Brazil, *Trans. R. Soc. Edinburgh: Earth Sci.*, *81*(3), 221–246.
Koutsoukos, E. A. M., P. N. Leary, and M. B. Hart (1990), Latest Cenomanian-earliest Turonian low-oxygen tolerant benthonic foraminifera: A case-study from the Sergipe basin (NE Brazil) and the western Anglo-Paris Basin (southern England), *Palaeogeogr. Palaeoclimatol. Palaeoecol.*, *77*(2), 145–177.
Kurtz, A., L. Kump, M. Arthur, J. Zachos, and A. Paytan (2003), Early Cenozoic decoupling of the global carbon and sulfur cycles, *Paleoceanography*, *18*(4), 1090, doi:10.1029/2003PA000908.
Linke, P., and G. Lutze (1993), Microhabitat preferences of benthic foraminifera—A static concept or a dynamic adaptation to optimize food acquisition?, *Mar. Micropaleontol.*, *20*(3), 215–234.
Lourens, L. J., A. Sluijs, D. Kroon, J. C. Zachos, E. Thomas, U. Röhl, J. Bowles, and I. Raffi (2005), Astronomical pacing of late Palaeocene to early Eocene global warming events, *Nature*, *435*(7045), 1083–1087.
Luciani, V., L. Giusberti, C. Agnini, E. Fornaciari, D. Rio, D. J. A. Spofforth, and H. Pälike (2010), Ecological and evolutionary response of Tethyan planktonic foraminifera to the Middle Eocene Climatic Optimum (MECO) from the Alano section (NE Italy), *Palaeogeogr. Palaeoclimatol. Palaeoecol.*, *292*(1–2), 82–95.
Lunt, D. J., A. Ridgwell, A. Sluijs, J. Zachos, S. Hunter, and A. Haywood (2011), A model for orbital pacing of methane hydrate destabilization during the Palaeogene, *Nat. Geosci.*, *4*, 775–778.
Lyle, M., A. O. Lyle, J. Backman, and A. Tripati (2005), Biogenic sedimentation in the Eocene equatorial Pacific – The stuttering greenhouse and Eocene carbonate compensation depth, *Proceedings of the Ocean Drilling Program: Scientific Results, ODP Leg 199*, 1–35.
Mackensen, A., H. Sejrup, and E. Jansen (1985), The distribution of living benthic foraminifera on the continental slope and rise off southwest Norway, *Mar. Micropaleontol.*, *9*(4), 275–306.
Mackensen, A., H. Grobe, and G. Schmiedl (1993), Benthic foraminiferal assemblages from the eastern South Atlantic Polar Front region between 35 and 57°S: Distribution, ecology and fossilization potential, *Mar. Micropaleontol.*, *22*(1), 33–69.
Maclennan, J., and S. M. Jones (2006), Regional uplift, gas hydrate dissociation and the origins of the Paleocene-Eocene Thermal Maximum, *Earth Planet. Sci. Lett.*, *245*(1), 65–80.
MacLeod, K. G., B. T. Huber, T. Pletsch, U. Röhl, and M. Kucera (2001), Maastrichtian foraminiferal and paleoceanographic changes on Milankovitch timescales, *Paleoceanography*, *16*(2), 133–154, doi:10.1029/2000PA000514.
Mancin, N., B. W. Hayward, I. Trattenero, M. Cobianchi, and C. Lupi (2013), Can the morphology of deep-sea benthic foraminifera reveal what caused their extinction during the mid-Pleistocene climate transition?, *Mar. Micropaleontol.*, *104*, 53–70.
Melki, T., N. Kallel, F. Jorissen, F. Guichard, B. Dennielou, S. Berné, L. Labeyrie, and M. Fontugne (2009), Abrupt climate change, sea surface salinity and paleoproductivity in the western Mediterranean Sea (Gulf of Lion) during the last 28 kyr, *Palaeogeogr. Palaeoclimatol. Palaeoecol.*, *279*(1), 96–113.
Miller, K. G., J. D. Wright, and R. G. Fairbanks (1991), Unlocking the Ice House: Oligocene-Miocene oxygen isotopes, eustasy, and margin erosion, *J. Geophys. Res.*, *96*(B4), 6829–6848, doi:10.1029/90JB02015.
Moebius, I., O. Friedrich, and H. D. Scher (2014), Changes in Southern Ocean bottom water environments associated with the Middle Eocene Climatic Optimum (MECO), *Palaeogeogr. Palaeoclimatol. Palaeoecol.*, *405*(1), 16–27.
Montero-Serrano, J. C., et al. (2011), Contrasting rainfall patterns over North America during the Holocene and Last Interglacial as recorded by sediments of the northern Gulf of Mexico, *Geophys. Res. Lett.*, *38*, L14709, doi:10.1029/2011GL048194.
Müller-Merz, E., and H. Oberhänsli (1991), Eocene bathyal and abyssal benthic foraminifera from a South Atlantic transect at 20-30°S, *Palaeogeogr. Palaeoclimatol. Palaeoecol.*, *83*(1–3), 117–171.
Murray, J. W. (2001), The niche of benthic foraminifera, critical thresholds and proxies, *Mar. Micropaleontol.*, *41*(1), 1–7.
Nicolo, M. J., G. R. Dickens, C. J. Hollis, and J. C. Zachos (2007), Multiple early Eocene hyperthermals: Their sedimentary expression on the New Zealand continental margin and in the deep sea, *Geology*, *35*(8), 699–702.
Norris, R., S. K. Turner, P. Hull, and A. Ridgwell (2013), Marine ecosystem responses to Cenozoic global change, *Science*, *341*(6145), 492–498.
Norris, R. D., D. Kroon, and A. Klaus (1998), Site 1051, *Proc. Ocean Drill. Program Initial Rep.*, *171B*, 171–239.
Nürnberg, D., M. Ziegler, C. Karas, R. Tiedemann, and M. W. Schmidt (2008), Interacting Loop Current variability and Mississippi River discharge over the past 400 kyr, *Earth Planet. Sci. Lett.*, *272*(1–2), 278–289.
Nyong, E. E., and R. Ramanathan (1985), A record of oxygen-deficient paleoenvironments in the Cretaceous of the Calabar Flank, SE Nigeria, *J. Afr. Earth Sci. (1983)*, *3*(4), 455–460.
Oberhänsli, H., E. Müller-Merz, and R. Oberhänsli (1991), Eocene paleoceanographic evolution at 20-30°S in the Atlantic Ocean, *Palaeogeogr. Palaeoclimatol. Palaeoecol.*, *83*(1), 173–215.
Ogg, J. E., and L. Bardot (2001), Aptian through Eocene magnetostratigraphic correlation of the Blake Nose Transect (Leg 171B), Florida continental margin, *Proc. Ocean Drill. Program Sci. Results*, *171B*, 58.
Pälike, H., M. W. Lyle, H. Nishi, I. Raffi, A. Ridgwell, K. Gamage, A. Klaus, G. Acton, L. Anderson, and J. Backman (2012), A Cenozoic record of the equatorial Pacific carbonate compensation depth, *Nature*, *488*(7413), 609–614.
Pearson, P. N., P. W. Ditchfield, J. Singano, K. G. Harcourt-Brown, C. J. Nicholas, R. K. Olsson, N. J. Shackleton, and M. A. Hall (2001), Warm tropical sea surface temperatures in the Late Cretaceous and Eocene epochs, *Nature*, *413*(6855), 481–487.
Pearson, P. N., B. E. van Dongen, C. J. Nicholas, R. D. Pancost, S. Schouten, J. M. Singano, and B. S. Wade (2007), Stable warm tropical climate through the Eocene epoch, *Geology*, *35*(3), 211–214.
Peryt, D., L. Alegret, and E. Molina (2002), The Cretaceous/Palaeogene (K/P) boundary at Aïn Settara, Tunisia: Restructuring of benthic foraminiferal assemblages, *Terra Nova*, *14*(2), 101–107.
Peterson, L., D. Murray, W. Ehrmann, and P. Hempel (1990), Cenozoic carbonate accumulation and compensation depth changes in the Indian Ocean, *Proceedings of the Ocean Drilling Program: Scientific Results, ODP Leg 115*, 311–333.

Petrová, P. (2004), Foraminiferal assemblages as an indicator of foreland basin evolution (Carpathian Foredeep, Czech Republic), *Bull. Geosci.*, *79*(4), 231–242.
Plattner, G. K., F. Joos, T. Stocker, and O. Marchal (2001), Feedback mechanisms and sensitivities of ocean carbon uptake under global warming, *Tellus, Ser. B*, *53*(5), 564–592.
Rasmussen, T. L., E. Thomsen, S. R. Troelstra, A. Kuijpers, and M. A. Prins (2003), Millennial-scale glacial variability versus Holocene stability: Changes in planktic and benthic foraminifera faunas and ocean circulation in the North Atlantic during the last 60,000 years, *Mar. Micropaleontol.*, *47*(1), 143–176.
Rasmussen, T. L., E. Thomsen, K. Skirbekk, M. Slubowska-Woldengen, D. Klitgaard Kristensen, and N. Koc (2014), Spatial and temporal distribution of Holocene temperature maxima in the northern Nordic Seas: Interplay of Atlantic-, Arctic- and polar water masses, *Quat. Sci. Rev.*, *92*, 280–291.
Renaudie, J., T. Danelian, S. Saint Martin, L. Le Callonnec, and N. Tribovillard (2010), Siliceous phytoplankton response to a middle Eocene warming event recorded in the tropical Atlantic (Demerara Rise, ODP Site 1260A), *Palaeogeogr. Palaeoclimatol. Palaeoecol.*, *286*(3–4), 121–134.
Rosoff, D. B., and B. H. Corliss (1992), An analysis of recent deep-sea benthic foraminiferal morphotypes from the Norwegian and Greenland Seas, *Palaeogeogr. Palaeoclimatol. Palaeoecol.*, *91*(1), 13–20.
Sarmiento, J. L., T. M. C. Hughes, R. J. Stouffer, and S. Manabe (1998), Simulated response of the ocean carbon cycle to anthropogenic climate warming, *Nature*, *393*(6682), 245–249.
Schmiedl, G., A. Mackensen, and P. Müler (1997), Recent benthic foraminifera from the eastern South Atlantic Ocean: Dependence on food supply and water masses, *Mar. Micropaleontol.*, *32*(3), 249–287.
Schoenfeld, J., and J. Burnett (1991), Biostratigraphical correlation of the Campanian-Maastrichtian boundary: Lägerdorf-Hemmoor (northwestern Germany), DSDP Sites 548A, 549 and 551 (eastern North Atlantic) with palaeobiogeographical and palaeoceanographical implications, *Geol. Mag.*, *128*(05), 479–503.
Sexton, P. F., P. A. Wilson, and R. D. Norris (2006), Testing the Cenozoic multisite composite d18O and d13C curves: New monospecific Eocene records from a single locality, Demerara Rise (Ocean Drilling Program Leg 207), *Paleoceanography*, *21*, PA2019, doi:10.1029/2005PA001253.
Sexton, P. F., R. D. Norris, P. A. Wilson, H. Pälike, T. Westerhold, U. Röhl, C. T. Bolton, and S. Gibbs (2011), Eocene global warming events driven by ventilation of oceanic dissolved organic carbon, *Nature*, *471*(7338), 349–352.
Shackleton, N. J., M. A. Hall, and A. Boersma (1984), Oxygen and carbon isotope data from Leg 74 foraminifers, *Proc. Deep Sea Drill. Proj. Initial Rep.*, *74*, 599–612.
Sluijs, A., S. Schouten, T. H. Donders, P. L. Schoon, U. Röhl, G.-J. Reichart, F. Sangiorgi, J.-H. Kim, J. S. S. Damsté, and H. Brinkhuis (2009), Warm and wet conditions in the Arctic region during Eocene Thermal Maximum 2, *Nat. Geosci.*, *2*(11), 777–780.
Sluijs, A., J. C. Zachos, and R. E. Zeebe (2012), Constraints on hyperthermals, *Nat. Geosci.*, *5*(4), 231.
Sluijs, A., R. E. Zeebe, P. K. Bijl, and S. M. Bohaty (2013), A middle Eocene carbon cycle conundrum, *Nat. Geosci.*, *6*(6), 429–434.
Smart, C. W., E. Thomas, and A. T. Ramsay (2007), Middle-late Miocene benthic foraminifera in a western equatorial Indian Ocean depth transect: Paleoceanographic implications, *Palaeogeogr. Palaeoclimatol. Palaeoecol.*, *247*(3), 402–420.
Spofforth, D. J. A., C. Agnini, H. Pälike, D. Rio, E. Fornaciari, L. Giusberti, V. Luciani, L. Lanci, and G. Muttoni (2010), Organic carbon burial following the Middle Eocene Climatic Optimum in the central western Tethys, *Paleoceanography*, *25*, PA3210, doi:10.1029/2009PA001738.
Stassen, P., C. Dupuis, E. Steurbaut, J. Yans, and R. P. Speijer (2012), Perturbation of a Tethyan coastal environment during the Paleocene/Eocene Thermal Maximum in Tunisia (Sidi Nasseur and Wadi Mezaz), *Palaeogeogr. Palaeoclimatol. Palaeoecol.*, *317*, 66–92.
Svensen, H., S. Planke, A. Malthe-Sørenssen, B. Jamtveit, R. Myklebust, T. R. Eidem, and S. S. Rey (2004), Release of methane from a volcanic basin as a mechanism for initial Eocene global warming, *Nature*, *429*(6991), 542–545.
Takeda, K., and K. Kaiho (2007), Faunal turnovers in central Pacific benthic foraminifera during the Paleocene-Eocene Thermal Maximum, *Palaeogeogr. Palaeoclimatol. Palaeoecol.*, *251*(2), 175–197.
Thomas, E. (1990), Late Cretaceous through Neogene deep-sea benthic foraminifers (Maud Rise, Weddell Sea, Antartica), *Proc. Ocean Drill. Program Sci. Results*, *113*, 571–594.
Thomas, E. (1998), Biogeography of the late Paleocene benthic foraminiferal extinction, in *Late Paleocene-Early Eocene Climatic and Biotic Events in the Marine and Terrestrial Records*, edited by M. P. Aubry, S. Lucas, and W. A. Berggren, pp. 214–243, Columbia Univ. Press, New York.
Thomas, E. (2003), Extinction and food at the seafloor: A high-resolution benthic foraminiferal record across the Initial Eocene Thermal Maximum, Southern Ocean site 690, *Geol. Soc. Am. Spec. Publ.*, *369*, 319–332.
Thomas, E., and N. J. Shackleton (1996), The Paleocene-Eocene benthic foraminiferal extinction and stable isotope anomalies, *Geol. Soc. London Spec. Publ.*, *101*(1), 401–441.
Thomas, E., J. C. Zachos, and T. J. Bralower (2000), Deep-sea environments on a warm Earth: Latest Paleocene-early Eocene, in *Warm Climates in Earth History*, edited by B. T. Huber, K. MacLeod, and S. Wing, pp. 132–160, Cambridge Univ. Press, Cambridge, U. K.
Thunell, R. C., and L. A. Reynolds (1984), Sedimentation of planktonic foraminifera: Seasonal changes in species flux in the Panama Basin, *Micropaleontology*, *30*(3), 243–262.
Tjalsma, R. C., and G. Lohmann (1983), Paleocene-Eocene bathyal and abyssal benthic foraminifera from the Atlantic Ocean, *Micropaleontol. Spec. Publ.*, *4*, 1–90.
Toffanin, F., C. Agnini, E. Fornaciari, D. Rio, L. Giusberti, V. Luciani, D. J. A. Spofforth, and H. Pälike (2011), Changes in calcareous nannofossil assemblages during the Middle Eocene Climatic Optimum: Clues from the central-western Tethys (Alano section, NE Italy), *Mar. Micropaleontol.*, *81*(1-2), 22–31.
Van der Zwaan, G., I. Duijnstee, M. Den Dulk, S. Ernst, N. Jannink, and T. Kouwenhoven (1999), Benthic foraminifers: Proxies or problems? A review of paleocological concepts, *Earth Sci. Rev.*, *46*(1-4), 213–236.
Van Kreveld, S. A. (1997), Northeast Atlantic late Quaternary planktic foraminifera as primary productivity and water mass indicators, *Oceanogr. Lit. Rev.*, *44*(7), 699–700.
Wade, B. S., D. Kroon, and R. D. Norris (2001), Orbitally forced climate change in late mid-Eocene time at Blake Nose (Leg 171B): Evidence from stable isotopes in foraminifera, *Geol. Soc. London Spec. Publ.*, *183*(1), 273–291.
Westerhold, T., U. Röhl, H. K. McCarren, and J. C. Zachos (2009), Latest on the absolute age of the Paleocene-Eocene Thermal Maximum (PETM): New insights from exact stratigraphic position of key ash layers +19 and −17, *Earth Planet. Sci. Lett.*, *287*(3), 412–419.
Widmark, J. G. V. (1995), Multiple deep-water sources and trophic regimes in the latest Cretaceous deep sea: Evidence from benthic foraminifera, *Mar. Micropaleontol.*, *26*(1), 361–384.
Widmark, J. G. V., and R. P. Speijer (1997), Benthic foraminiferal faunas and trophic regimes at the terminal Cretaceous tethyan seafloor, *Palaios*, *12*(4), 354–371.
Winguth, A. M. E., E. Thomas, and C. Winguth (2012), Global decline in ocean ventilation, oxygenation, and productivity during the Paleocene-Eocene Thermal Maximum: Implications for the benthic extinction, *Geology*, *40*(3), 263–266.

Witkowski, J., S. M. Bohaty, K. McCartney, and D. M. Harwood (2012), Enhanced siliceous plankton productivity in response to middle Eocene warming at Southern Ocean ODP Sites 748 and 749, *Palaeogeogr. Palaeoclimatol. Palaeoecol.*, *326*, 78–94.

Witkowski, J., S. M. Bohaty, K. M. Edgar, and D. M. Harwood (2014), Rapid fluctuations in mid-latitude siliceous plankton production during the Middle Eocene Climatic Optimum (ODP Site 1051, western North Atlantic), *Mar. Micropaleontol.*, *106*, 110–129.

Zachos, J. C., T. M. Quinn, and K. A. Salamy (1996), High-resolution (104 years) deep-sea foraminiferal stable isotope records of the Eocene-Oligocene climate transition, *Paleoceanography*, *11*(3), 251–266, doi:10.1029/96PA00571.

Zachos, J. C., M. Pagani, L. Sloan, E. Thomas, and K. Billups (2001), Trends, rhythms, and aberrations in global climate 65 Ma to present, *Science*, *292*(5517), 686–693.

Zachos, J. C., M. W. Wara, S. Bohaty, M. L. Delaney, M. R. Petrizzo, A. Brill, T. J. Bralower, and I. Premoli-Silva (2003), A transient rise in tropical sea surface temperature during the Paleocene-Eocene Thermal Maximum, *Science*, *302*(5650), 1551–1554.

Zachos, J. C., G. R. Dickens, and R. E. Zeebe (2008), An early Cenozoic perspective on greenhouse warming and carbon-cycle dynamics, *Nature*, *451*(7176), 279–283.

Zachos, J. C., H. McCarren, B. Murphy, U. Röhl, and T. Westerhold (2010), Tempo and scale of late Paleocene and early Eocene carbon isotope cycles: Implications for the origin of hyperthermals, *Earth Planet. Sci. Lett.*, *299*(1), 242–249.